Statistical property parameterization of simple rocking block response

Christos G. Lachanas,[1*] Dimitrios Vamvatsikos,[1] Elias G. Dimitrakopoulos[2]
[1] *School of Civil Engineering, National Technical University of Athens, Athens, Greece.*
[2] *Department of Civil and Environmental Engineering, The Hong Kong University of Science and Technology, Clear Water Bay, Hong Kong, People's Republic of China.*

Summary

The parametric representation of rocking fragilities is statistically investigated. Initially, the potential normalization of the rocking parameters to reduce the problem's dimensionality is tackled by undertaking comparisons both on a single-record and a sample-of-records basis. It is found that the slenderness angle can be normalized out when probabilistically considering the rocking response of simple rocking blocks with the same semi-diagonal length. Then, the robustness of the lognormal distribution for characterizing the rocking motion is investigated. Sets of pulse-like and ordinary ground motions are employed to test the lognormal fit for the full range of rocking response when the peak ground acceleration or the peak ground velocity are employed as intensity measures. In both cases, the lognormal distribution offers an adequate, but often imperfect, baseline model of the rocking fragility curves. Instead, a shifted lognormal that accounts for the absence of response below the rocking initiation intensity is an enhanced solution that can form the basis for offering simplified response model surrogates.

KEYWORDS
incremental dynamic analysis, rigid rocking blocks, seismic demands, response statistics

1 INTRODUCTION

Rocking is a common pattern of seismic response for unanchored rigid bodies subjected to earthquake excitation. In general, sliding, bouncing or a mixed response may occur. Yet, when the coefficient of friction between block's base and its support surface is high enough to prevent sliding, and the block is sufficiently slender to prevent bouncing [1], it undergoes pure rocking during an earthquake motion. Housner in 1963 [2] proposed the rocking equation of motion. Numerous studies followed on the analytical investigation of the rocking response under single-pulses or earthquake ground motion excitations [e.g. 3–16]. This interest in the field of rocking stems from its wide application in structures. The rocking block has been employed for the determination of the seismic response for a wide range of structural types starting from ancient temples or monuments [e.g. 9, 17–20] to the design of modern and resilient structures [e.g., 21–24]. Most of the aforementioned studies investigate the rocking problem via analytical treatments aiming to determine the correlation between the excitation's waveform characteristics and the block's geometric and dynamic characteristics. Such efforts are motivated by, but are also hampered by, the extreme nonlinearity of the rocking motion, which is strongly dependent on the initial conditions [3]. This naturally leads to the consideration of the probabilistic assessment as an efficient approach. Yim *et al*. [3] and recently Voyagaki and Vamvatsikos [25] undertook the probabilistic treatment of the uncertainties that are associated with the rocking problem in a similar way with the treatment of the uncertainty sources that are involved in the seismic response of yielding systems. A statistical approach to the rocking response is also presented by Bachmann *et al.* [16] where a validation of Housner's simple rocking model [2] for the efficient prediction of the response statistics is provided. Moreover, recent shake table testing campaigns [26] targeted the statistical characteristics of the response instead of the response under single ground motions since rocking response cannot be efficiently predicted by virtue of being strongly dependent on the modeling details [27].

The probabilistic treatment is also the common tool for producing predictive equations for the seismic response of structural systems [28–31]. These empirically-derived expressions are used for the rapid estimation of the (distribution of the) seismic demand and are produced by regressing the results of thousands or millions of dynamic analyses of simplified models, typically equivalent single-degree-of-freedom systems. Reducing the size of (i) the input parameter space and (ii) of the output statistical metrics is an obvious bonus to such endeavors. The first can be achieved by normalizing out the system parameters and reducing them to the absolute minimum number required by the dimensionality of the problem. The second is best managed by adopting a parametric probability distribution that efficiently fits the system response or, equivalently, captures the system fragility function(s) [32]. A widely accepted solution has already been reached on how to tackle such issues for elastoplastic hysteretic oscillators by adopting the triptych of strength-ratio/ductility/period to characterize the system [28,33], together with a lognormal distribution to capture the response [29, 30]. Such consensus is still lacking for the simple rocking block.

* Corresponding author: lahanasch@central.ntua.gr

In an attempt to propose a comprehensive resolution, a detailed discussion is provided on the parameterization of rocking response and on the use of a common distribution model for fitting the rocking fragilities. Dimensional analysis has already made strong contributions to the first issue, although mostly confined to pure-pulse excitation [10]. Whether such normalized parameters are also applicable for recorded (pulse-like or non-pulse-like) ground motions remains a question. There is even less information for selecting a response distribution model. The lognormal is a typical, albeit imperfect, assumption for yielding systems. For example, Romão *et al.* [34] recommend a lognormal distribution for the distribution of most engineering demand parameters (EDPs) given the intensity measure (IM) level, at least where non-collapsing response is concerned. On the other hand, Goda *et al.* [35] recommend either the lognormal or the Frechet distribution for different cases of non-collapsing systems with Bouc-Wen hysteresis. Where collapse (or block overturning) starts appearing, at least two distributions are needed for the EDP given IM data [13]. Instead, characterization of response via a single common distribution model is still feasible for the fragilities, or equivalently, for the IM given EDP data. For example, Shinozuka *et al.* [36] suggest the lognormal distribution for yielding system fragilities. The question is whether this is also fine for rocking response, or a different distribution model is needed.

The present work is part of a series of papers [31, 37–40] that aim to investigate in detail the seismic response standardization for the case of rigid rocking blocks via state-of-the-art probabilistic approaches in order to offer practical tools to predict the (distribution of) rocking response for the seismic design and assessment of on-ground or floor-supported rocking blocks. All these tools can be applied for cases of individual blocks or in modern decision support systems [e.g., 41] for treating multiple assets of rocking response.

2 THE SIMPLE ROCKING BLOCK AND ITS PROPERTIES

Rocking fundamentals

The classic rocking block problem refers to a planar rigid block (Figure 1), rocking without sliding or bouncing on a rigid base subjected to horizontal excitation. Customarily, the block is rectangular with $2b$ base width and $2h$ total height. Rocking motion starts once the overturning moment of the seismic force overcomes the restoring moment of gravity. The corresponding horizontal acceleration condition is $\ddot{u}_g > \mathrm{g}\tan\alpha$.

After uplifting, the block rocks between its pivot points O and O'. The rocking motion between impacts can be described by the single degree of freedom equation [11]:

$$\ddot{\theta} = -p^2\left[\sin(\alpha\mathrm{sgn}(\theta) - \theta) + \frac{\ddot{u}_g}{\mathrm{g}}\cos(\alpha\mathrm{sgn}(\theta) - \theta)\right] \tag{1}$$

where θ is the rocking angle, $\alpha = \tan^{-1}(b/h)$ the slenderness (or stability) angle, and p is the characteristic frequency parameter of the block, which for a rectangular block is $p = \sqrt{(3\mathrm{g})/(4\mathrm{R})}$, with $R = \sqrt{b^2 + h^2}$ being the half diagonal of the block. Equation (1) is valid for large θ rotations and slenderness angles α. For small θ and α, Equation (1), simplifies to [14]:

$$\frac{\ddot{\theta}(t)}{p^2\alpha} - \frac{\theta(t)}{\alpha} + \mathrm{sgn}(\theta) = -\frac{\ddot{u}_g}{\mathrm{g}\alpha} \tag{2}$$

In Equations (1) and (2) note the negative sign in front of θ, which implies negative stiffness, and that there is no damping term. Energy dissipation occurs mainly during the impact of the block to its support base during rocking response. Impacts take place at the pivot points (θ = 0), when the rocking rotation θ switches sign ($\mathrm{sgn}(\theta) = \pm 1$). A common way to capture this energy loss is with a coefficient of restitution η. Typically, η is defined as the ratio of post $\dot{\theta}^+$ and pre-impact $\dot{\theta}^-$ angular velocity:

$$\eta = \frac{\dot{\theta}^+}{\dot{\theta}^-} \tag{3}$$

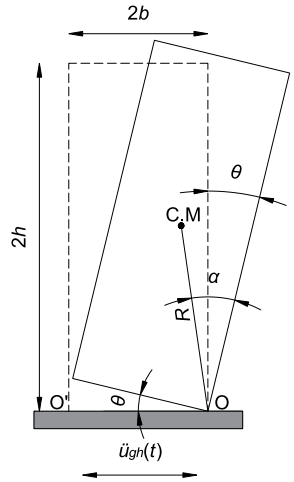

Figure 1. Planar rectangular rocking block on a rigid base.

Housner [2] proposed an approximation for the coefficient of restitution based on the conservation of angular moment before and after the impact: $\eta = 1 - (3/2)\sin^2(\alpha)$. However, this estimate associates the energy dissipation at impact only with the block shape (slenderness angle α) and disregards all remaining factors that are involved in the impact itself such as the material properties, the foundation etc. Typically, the value of the coefficient of restitution η ranges within 0.7–1.0 [e.g., 42–46].

Ultimately, rocking motion terminates with the block either returning to rest or with overturning. Mathematically, overturning occurs if the (absolute) rocking rotation diverges to infinity $|\theta| \to \infty$. Numerically, overturning is assumed once the rocking rotation exceeds an arbitrarily large value, e.g., $|\theta| > \pi/2$ or $|\theta| > \alpha$, both options providing statistically identical results.

Parameters and variables of the rocking problem

Despite the structural simplicity of the rocking block, its dynamic behavior is nonlinear and very sensitive to the waveform of the ground motion. The parameters governing the motion of the rocking block are three:

1. A geometrical characteristic of the block related to its shape: the slenderness angle α.
2. The frequency parameter p, which is associated with the size of the block through the value of the diagonal $2R$. Recall that the "equivalent" oscillation frequency of rocking response depends both on p and on the rocking amplitude [1] and hence cannot be directly compared to the natural frequency of the yielding oscillators [8].
3. The coefficient of restitution η, which refers to the energy loss mechanism during the rocking motion. The energy dissipation mechanism is a fundamental difference between rocking and the typical yielding single-degree-of-freedom (SDOF) system (see [8] and references therein). There are three common ways of approaching the value of η. The first and relatively impractical option is the case-specific experimental determination of η. The second and most commonly employed is the slenderness-dependent equation of Housner [2]. In that case, the slenderness angle α is involved in the η calculation. The third option is to employ a constant value for η that is independent of α [47, 48]; this is the approach of the present analysis. This constant value assumption is based on the moderate effect that η is found to have, in a statistical sense, in comparison with the other system parameters [3, 16, 48], as well as, on the aforementioned issues regarding an effective direct estimation.

Note that the mass of the block is not a governing parameter of the classical rocking block problem. Instead, there are two parameters referring to the geometrical characteristics of the block (α and p) while the third (η) refers to the energy loss during the impact. Crucially, despite the superficial differences, the same three parameters govern the response of any single-degree of freedom (SDOF) (rigid) rocking mechanisms, as there is a direct equivalence between different SDOF rocking structures [49].

In addition to the three block-specific parameters, to achieve full characterization one must also introduce two analysis-specific variables: The ground motion intensity, represented by the scalar intensity measure (IM), and the engineering demand parameter (EDP) capturing the structural response. Typical IMs for rocking blocks are the peak ground acceleration (PGA), and the peak ground velocity (PGV) [13, 50, 51]. As the EDP, one usually employs the peak absolute rocking angle recorded, θ_{max}.

Having a total of five (three plus two) quantities that need to be accounted for, one wonders what can be normalized out. The assumption of a constant coefficient of restitution η already removes one. Dimensional analysis offers further options via the normalization of the IM and the EDP, at least for pure-pulse excitations and slender blocks (e.g., α < 0.20 rad) [10]. For this particular case, one can remove the effect of α by adopting as EDP the dimensionless peak rocking angle $\tilde{\theta} = \theta_{max}/\alpha$, and as dimensionless IM either $PGA/(\mathrm{g}\tan\alpha)$, denoted here as $PGA/\mathrm{g}\tan\alpha$, or $(pPGV)/(\mathrm{g}\tan\alpha)$, denoted here as $pPGV/\mathrm{g}\tan\alpha$. Unfortunately, the degree to which such treatments are effective is a matter of debate. At the highest level, one would require that this double IM and EDP normalization would make the full response histories identical under a given excitation. For a simple sinusoidal pulse excitation and slender blocks of the same *p*, this is indeed the case [10]. For realistic pulse-like ground motions, the resulting response histories are close but not the same [13, 14], while no data is available for non-pulse-like ground motions. At a second level, having a matching of just the maximum response, $\tilde{\theta}$, under a given ground motion record would be adequate. Actually, one can lower his/her requirements to a third level by only seeking the matching of the distribution statistics of $\tilde{\theta}$ given the IM under a suite of ground motions. If any of the above matchings is valid, the slenderness (or stability) angle α can be effectively removed from the problem, especially when undertaking a probabilistic view of rocking as, for example, when seeking the determination of fragility curves, as e.g. proposed by Kazantzi et al. [31, 39].

3 CASE STUDY SETUP

In order to check the effectiveness of normalization by the slenderness (or stability) angle α, a total number of 15 blocks are used. They have three different frequency values, p = 1.00, 3.00, 4.00 s^{-1}, and five different α ratios, ranging from very slender blocks with α = 0.05 rad to semi-stocky ones with α = 0.25 rad (Table 1). For the block slenderness angles employed, Housner's coefficient of restitution varies within $\eta \cong 0.91 - 1.00$. In the following, a constant coefficient of restitution value of $\eta = 0.92$ is employed for all blocks [31, 39, 47, 48] that translates into an energy loss of 15.36% per impact.

Table 1. Geometric and dynamic characteristics of the 5×3 studied blocks.

p (s^{-1})	1.00			3.00			4.00		
α (rad)	2b (m)	2h (m)	R (m)	2b (m)	2h (m)	R (m)	2b (m)	2h (m)	R (m)
0.05	0.735	14.697	7.358	0.082	1.633	0.818	0.046	0.919	0.460
0.10	1.469	14.641	7.358	0.163	1.627	0.818	0.092	0.915	0.460
0.15	2.199	14.550	7.358	0.244	1.617	0.818	0.137	0.909	0.460
0.20	2.923	14.422	7.358	0.325	1.602	0.818	0.183	0.901	0.460
0.25	3.641	14.258	7.358	0.405	1.584	0.818	0.228	0.891	0.460

Multiple nonlinear dynamic analyses are performed using the simplified Housner [2] model. Specifically, all the analyses integrate numerically Equation (1) using scripts developed by Vassiliou [52]. This simplified approach of a planar rigid block undergoing pure rocking response may lack in accuracy in comparison with more sophisticated models. However, as proposed by Bachmann *et al.* [16], it remains a highly efficient approach for probabilistically investigating rocking response, which requires hundreds or thousands of nonlinear response history analyses. Natural recorded ground motions are used, all taken from the PEER NGA database [53]. Both pulse-type [54] and ordinary (no-pulse-like, no-long-duration) ground motions are employed for analyses either on a single-record or on sets-of-records basis via incremental dynamic analysis (IDA) [55]. All the records have *PGA* higher than 0.14 g and correspond to seismic events with moment magnitude higher than 6.2. These criteria allowed us to find records that can trigger rocking when unscaled even for the less slender blocks, while they reduce the scaling factors needed during IDA to capture overturning.

The methodology of rocking IDA proposed by Lachanas and Vamvatsikos [37] is employed. In all cases a constant *PGA* step of 0.01 g is employed for scaling. Incrementing stops at the first sign of overturning (i.e., $\theta \geq \alpha$), discarding any possible resurrections. This no-resurrection assumption is adequate for all practical purposes, as resurrections only matter for the response of sturdy blocks close to overturning [37]. Two record sets are used: one of 86 ordinary ground motions and another of 44 pulse-type ones [54], each with two horizontal components. From each pair, only one arbitrary horizontal component is employed. Correspondingly, both IMs of *PGA* and *PGV* are used in their arbitrary-component form: they are defined on the (arbitrarily selected) single horizontal component that is actually applied to the response history analysis of each block. Note that this has no bearing on the

conclusions, as similar observations are derived if the geomean IM values are used instead; these results are not shown here for brevity.

4 CAN WE NORMALIZE OUT THE SLENDERNESS?

A four-stage comparison is undertaken to clarify if the seismic response of blocks with the same size (p) but different shape (α) yields a unique response under dimensionless IM and EDP. It starts from (i) the single record full rocking response history, then progressively escalates to comparing (ii) a single IDA curve, (iii) sample statistics of IDA results calculated for entire record sets, and, finally, ends up by comparing (iv) the classic IDA approach of scaling the record amplitude versus the alternative of scaling the block slenderness. This staged comparison aims to uncover the effect of shape on the dimensionality of rocking response under both ordinary and pulse-like ground motions, starting from the deterministic and moving to the sample statistical view.

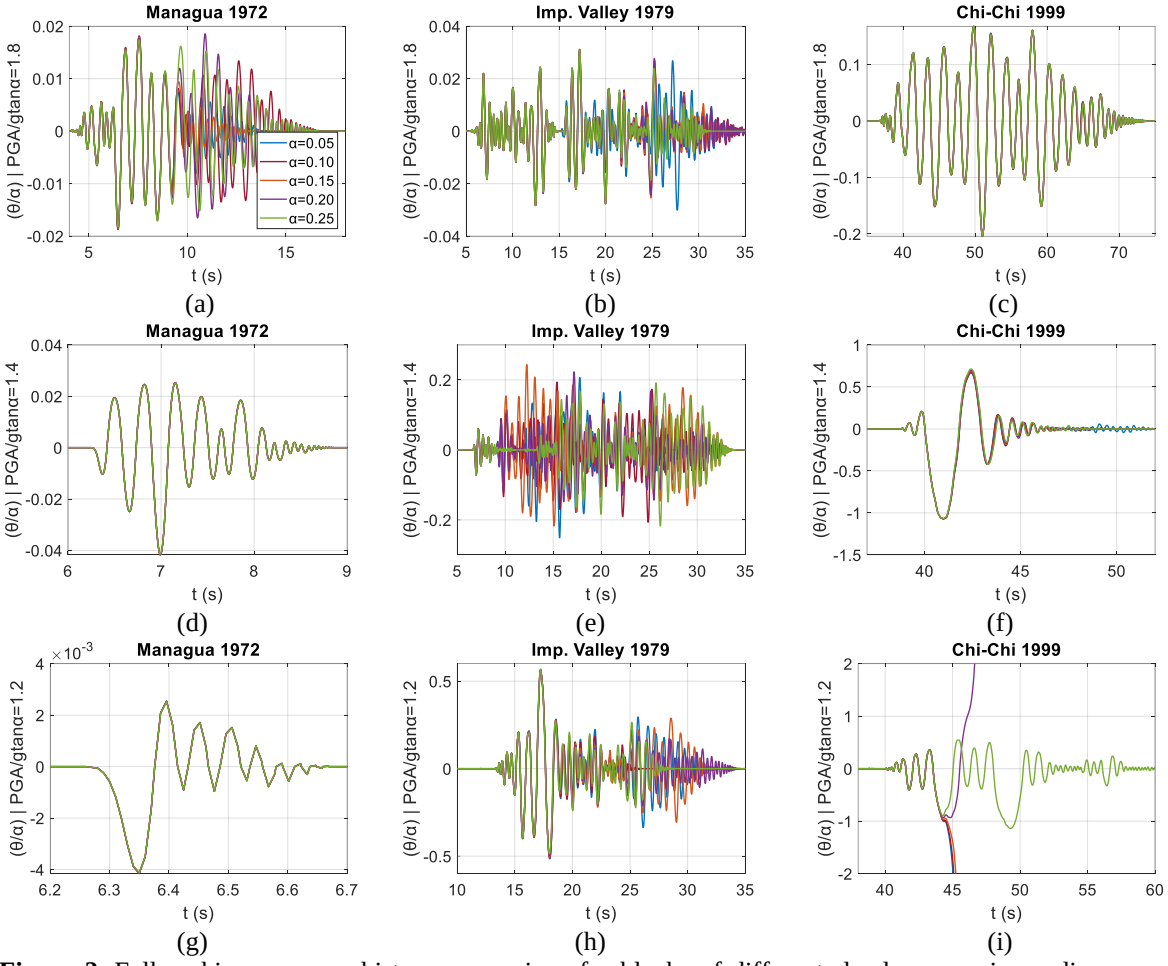

Figure 2. Full rocking response history comparison for blocks of different slenderness using ordinary ground motions scaled at the same normalized $PGA/\mathrm{g}\tan\alpha$ level per block: (a)-(c) blocks with p = 1 s^{-1}, (d)-(f) blocks with p = 3 s^{-1}, (g)-(i) blocks with p = 4 s^{-1}. Note that dissimilar axes have been used to enhance resolution.

Single response-history comparison

The first stage of comparison refers to the full rocking response history. To this end, by taking the 5×3 blocks of Table 1, the full rocking response history under single ground motions is compared. In order to assure rocking even for the less slender blocks of Table 1, ground motions are scaled to intensities of $PGA/\mathrm{g}\tan\alpha > 1$. As an example, the results for three ordinary (Figure 2) and three pulse-like (Figure 3) ground motions are shown. Different intensity levels per p case in Figures 2, 3 are selected to correspond mainly to $PGA/\mathrm{g}\tan\alpha$ levels where all blocks start rocking (and in their majority without reaching overturning) in order to investigate the matching of the rocking response waveform in the entire excitation time history. In general, the results are mixed and cannot support a definitive conclusion. Considering the ordinary non-pulsive records of Figure 2, normalization fails to produce an identical rocking time history for most of the cases. Still, relatively low differences are observed for

the peak dimensionless rocking angle in all cases. Even for the seemingly least compliant case of Chi-Chi 1999 record for p = 4 s^{-1} (Figure 2i), three blocks agree in overturning and only one diverges by surviving. This observation hints at what we expect to see in the next stages of comparison, having a mostly consistent matching response with only a few discrete outliers. On the other hand, for the case of pulse-like ground motions (Figure 3) normalization of the slenderness seems to work better even if not perfectly. The inherent pulse of the ground motion that dominates the response leads to better matching of the response history waveforms. However, there are still cases where normalization fails to produce identical response (i.e. Figure 3d).

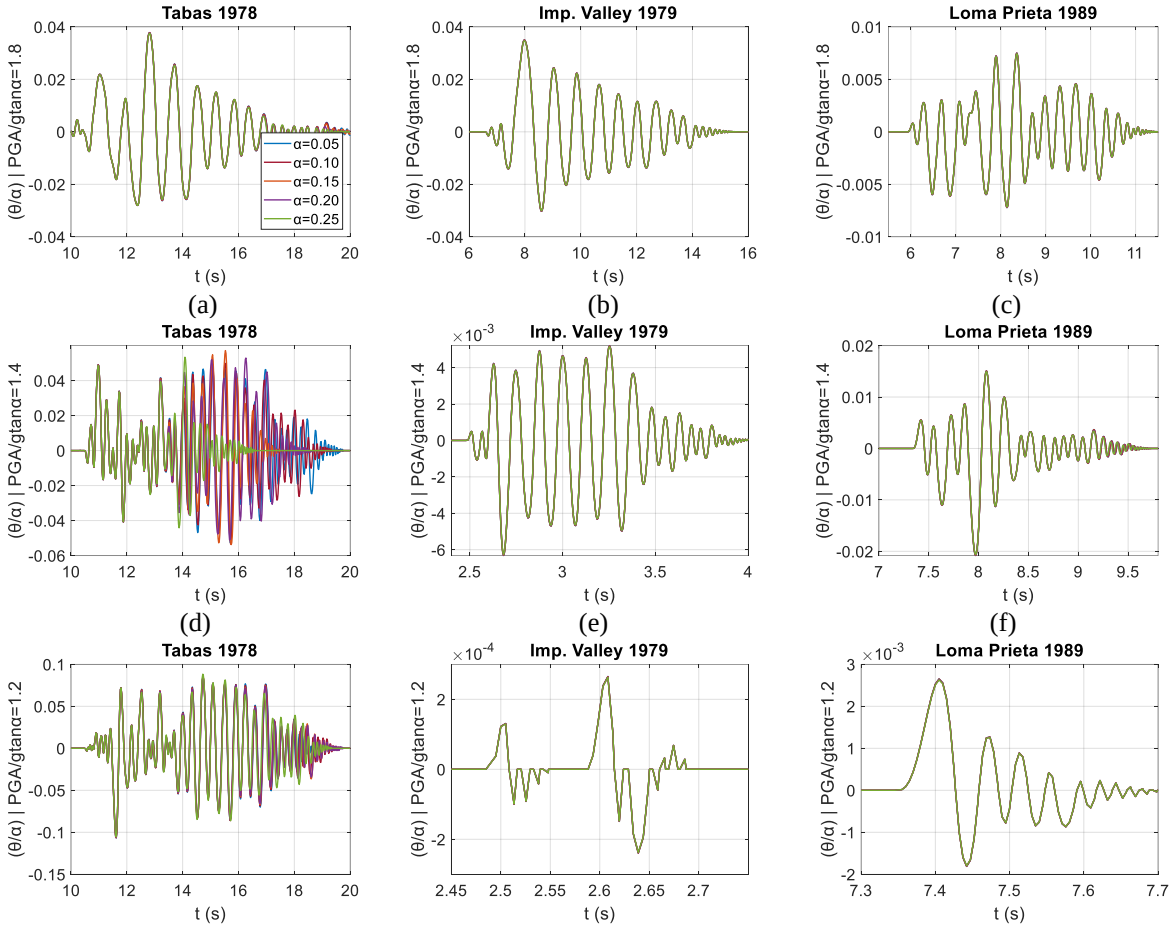

Figure 3. Full rocking response history comparison for blocks of different slenderness using pulse-type [54] ground motions scaled at the same normalized $PGA/\mathrm{g}\tan\alpha$ level per block: (a)-(c) blocks with p = 1 s^{-1}, (d)-(f) blocks with p = 3 s^{-1}, (g)-(i) blocks with p = 4 s^{-1}. Note that dissimilar axes have been used to enhance resolution.

Single IDA curve comparison

In the second stage, the comparison turns to the single record IDA curves. The difference of this stage with the previous is that now only the dimensionless peak rocking angle is considered instead of the full response history. The individual IDA curves allow us to efficiently examine this peak response at different levels of intensity. The same ordinary and pulse-type ground motions as in the previous section are used. As illustrated in Figure 4, for the ordinary ground motions some differences are still captured. These range from marginal, especially at low IM levels, to notable for a few instances of higher IMs, where some blocks manage to survive and some do not (see Figures 4b, 4d, 4e). On the other hand, when looking at the single IDA curves under pulse-like ground motions in Figure 5 the normalization seems to be very effective. As observed, for all the ground motions and the frequency cases, the seismic response of the blocks of different α yields close to a unique IDA curve in the dimensionless IM-EDP space. Only some minor differences are captured in some rare cases (i.e. Figure 5b), but these are well within the margin of what could be considered as acceptable, both for the curves of Figure 5 and for those not shown for brevity. Thus, when pulse-type ground motions are employed and only the peak response is of interest, there is little question that slenderness can be efficiently normalized out. In contrast, for the case of the ordinary ground motions, the differences observed necessitate further investigation.

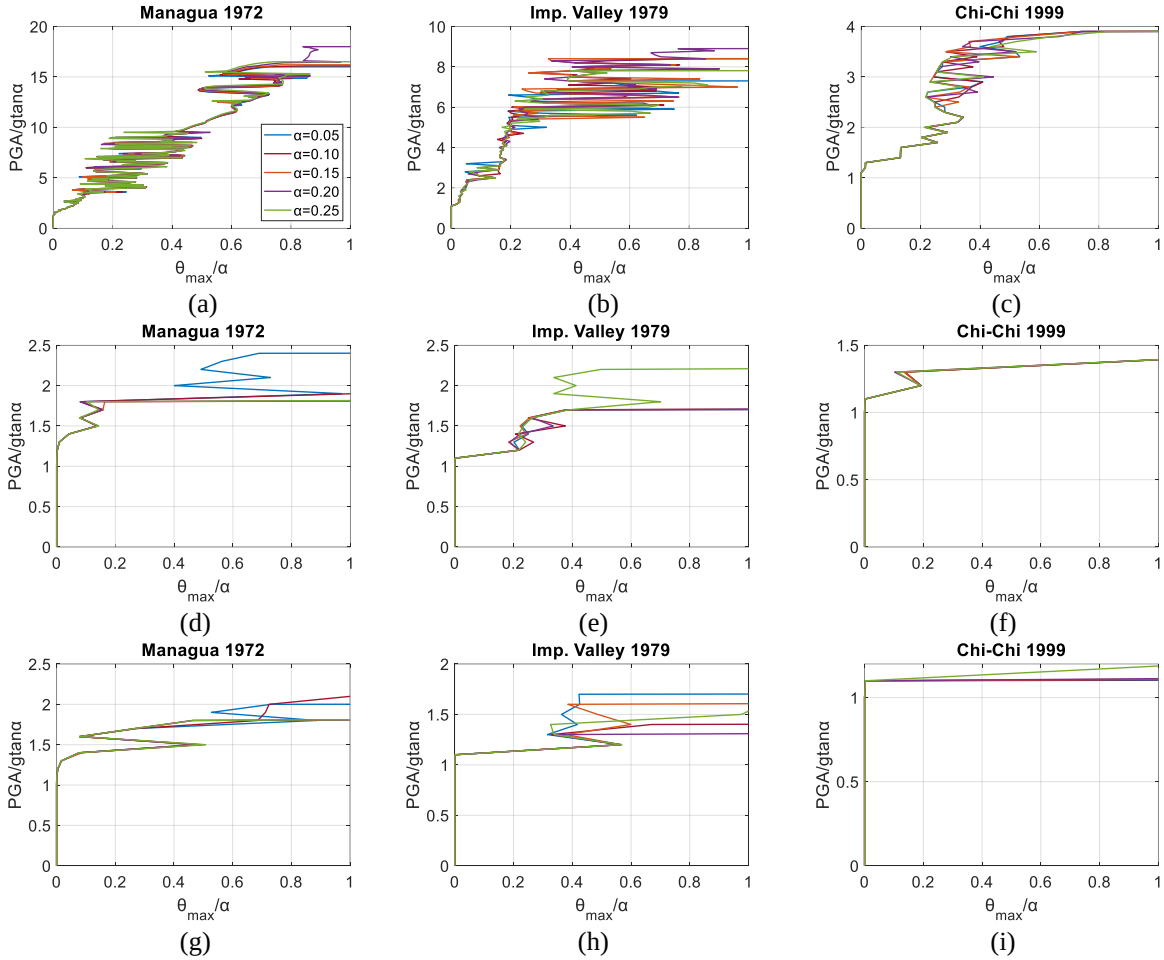

Figure 4. Single IDA curve comparison for blocks of different slenderness for ordinary ground motions: (a)-(c) blocks with p = 1 s^{-1}, (d)-(f) blocks with p = 3 s^{-1}, (g)-(i) blocks with p = 4 s^{-1}.

Full IDA statistics comparison

The third stage of comparison considers the peak response statistics at given levels of intensity. In this section, only the set of 86 ordinary ground motions is employed since for the pulse-type ones the efficiency of stability angle's normalization has already been verified at a higher level of compliance.

The comparison is made on two alternative bases for the estimated statistics. The first and stricter comparison is made on a paired-record basis [38]. In the context of medical studies, this corresponds to supplying the tested medicine versus a placebo (or two different α values) to identical twins (or records). Specifically, after the analysis with the full set of 86 ground motions for the 5×3 blocks of Table 1, a paired one-by-one record comparison is employed between blocks with the same p but different α. Specifically, for given levels of the dimensionless IM (i.e., horizontal stripes) we calculate the ratio of the response of each block of different slenderness angle (α) over the response of the $\alpha = 0.10$ rad block for each of the 86 records:

$$r_\alpha = \frac{\tilde{\theta}_\alpha}{\tilde{\theta}_{0.10}} \tag{4}$$

where $\tilde{\theta}_\alpha$ is the $\tilde{\theta}$ value of the record for the block with slenderness α, and $\tilde{\theta}_{0.10}$ the $\tilde{\theta}$ value of the same record at the same IM-level for the block with $\alpha = 0.10$ rad, both blocks having the same p.

Results via Equation (4) are plotted in the boxplots [56] of Figures 6–7 for various IM-levels. Only the well-defined ratios of the 86 records per stripe are considered. By this we mean ratios r_α where none of the two compared blocks overturns. As overturning becomes more frequent with higher intensities, this effect manifests itself in Figures 6–7 via the decreasing percentage of usable ratios with increasing intensity. Looking at each stripe's boxplot, the central mark denotes the median of r_α, the notches capture the 95% confidence interval for

the median, whereas the left and right edges of the block are the 25-75% percentiles of the sample. Whiskers are set equal to 1.5 times the 25-75% interquartile range whereas the observations beyond the whiskers are considered as outliers and are denoted with cross line symbols.

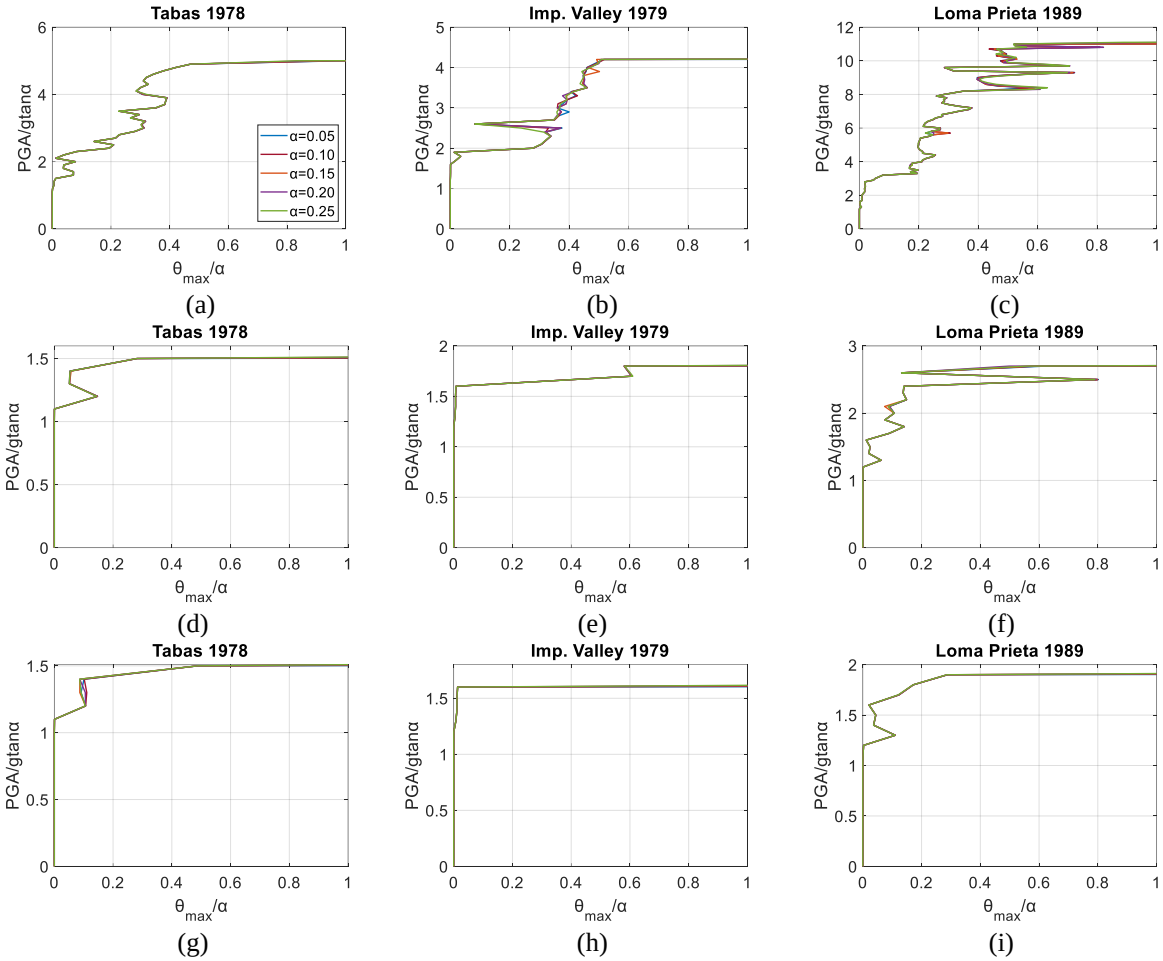

Figure 5. Single IDA curve comparison for blocks of different slenderness for pulse-type [54] natural records: (a)-(c) blocks with p = 1 s^{-1}, (d)-(f) blocks with p = 3 s^{-1}, (g)-(i) blocks with p = 4 s^{-1}.

Figure 6 captures the boxplots for the case of the blocks with p = 1 s^{-1}. As shown, the median r_α conforms to 1.0 with 95% confidence for most of the blocks and IM levels. The only exception regards the block with α = 0.25 rad in the lowest IM-stripe. The same tendency is observed for the blocks with p = 3 or 4 s^{-1} as presented in Figure 7. In general, even these small mismatches are of little practical consequence, as they concern small-amplitude response values close to uplift. Thus, taking their ratio can easily exaggerate the difference of otherwise relatively close values. Overall, at all intensity levels we can observe the existence of outliers where the responses of blocks with different α do not match, thus confirming our stage-two observations. Still, these are clearly the exception and not the rule. The vast majority conform to a ratio of 1.0. This conclusion seems to stand uniformly for the slender blocks, whereas for the less slender (semi-stocky) ones, even the small differences that are observed in the low IM levels may question the absolute efficiency of the normalization. Note that the same observations are valid if the comparison is employed on a vertical-statistics basis [32], i.e. for given EDP levels [37], the results of which are not shown here for reasons of brevity.

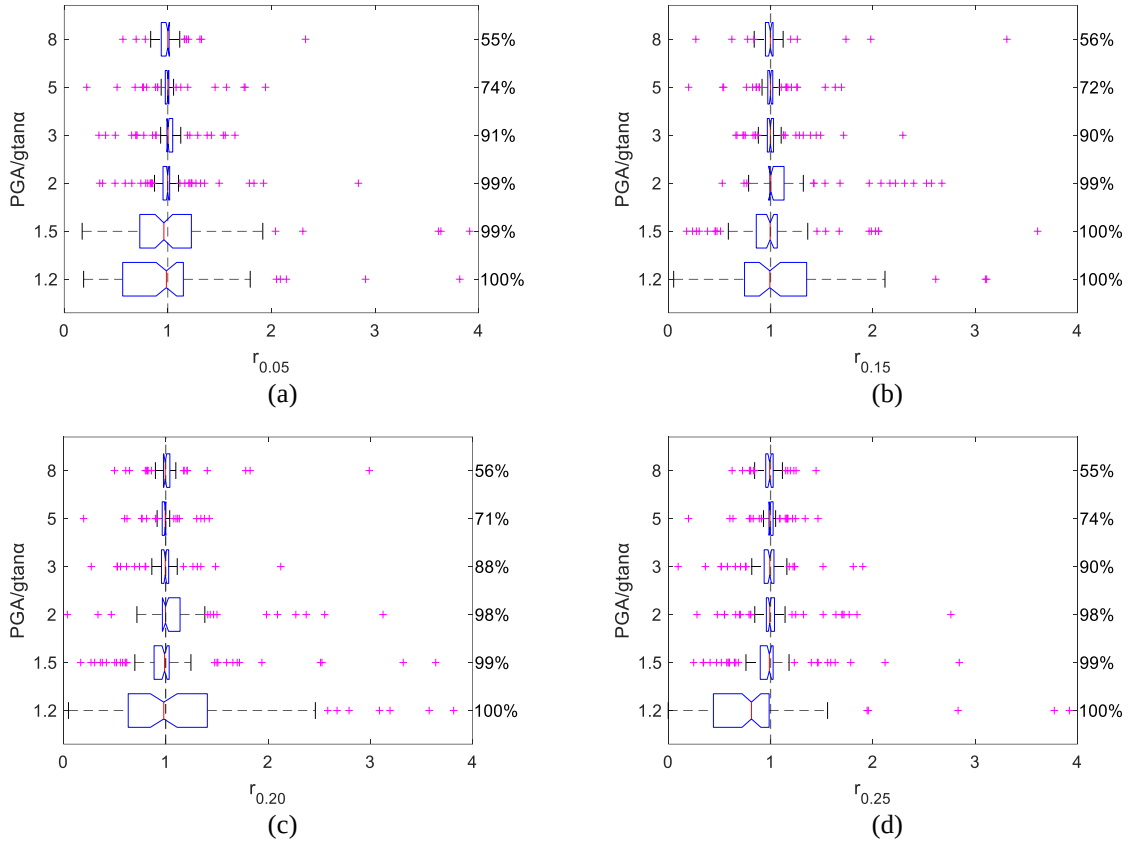

Figure 6. Boxplots of the ratio of response via Equation (4) for blocks with p = 1 s^{-1}. The percentage of non-infinite ratios from 86 total appears on the right vertical edge for each intensity level.

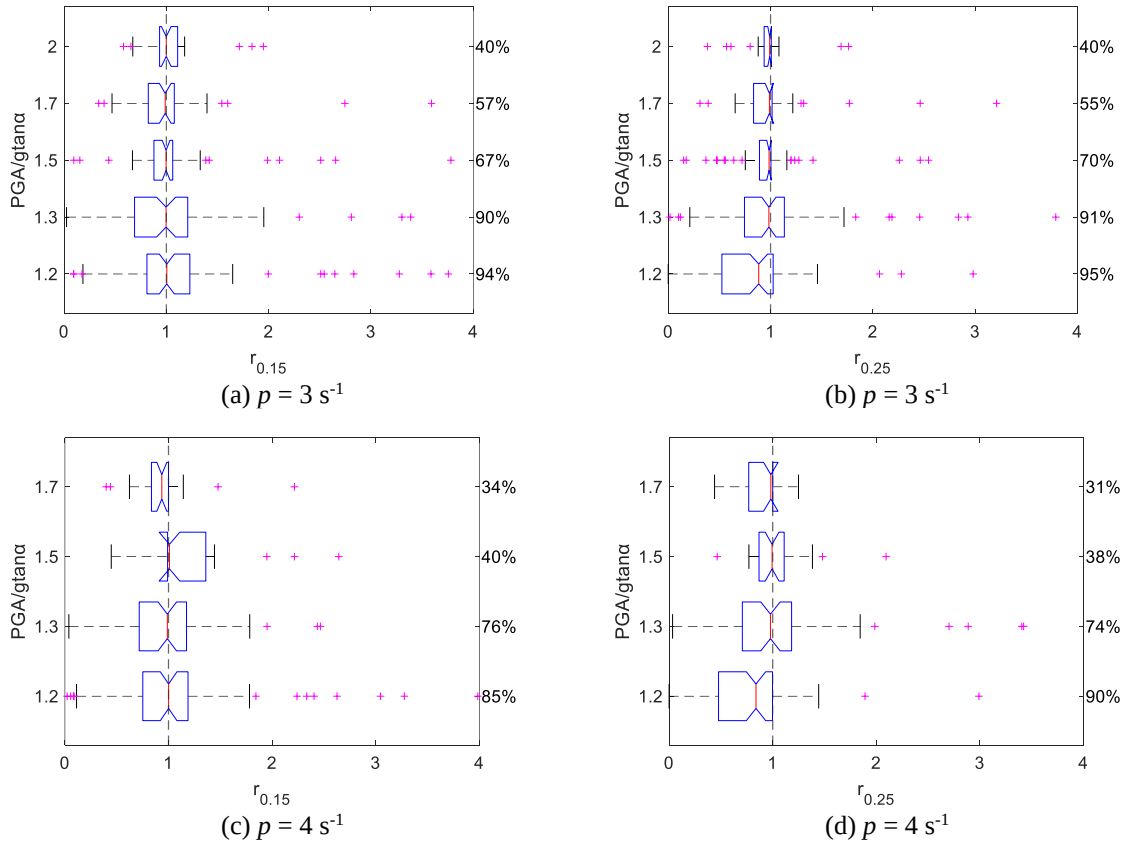

Figure 7. Boxplots of the ratio of response via Equation (4). The percentage of non-infinite ratios from 86 total appears on the right vertical edge for each intensity level.

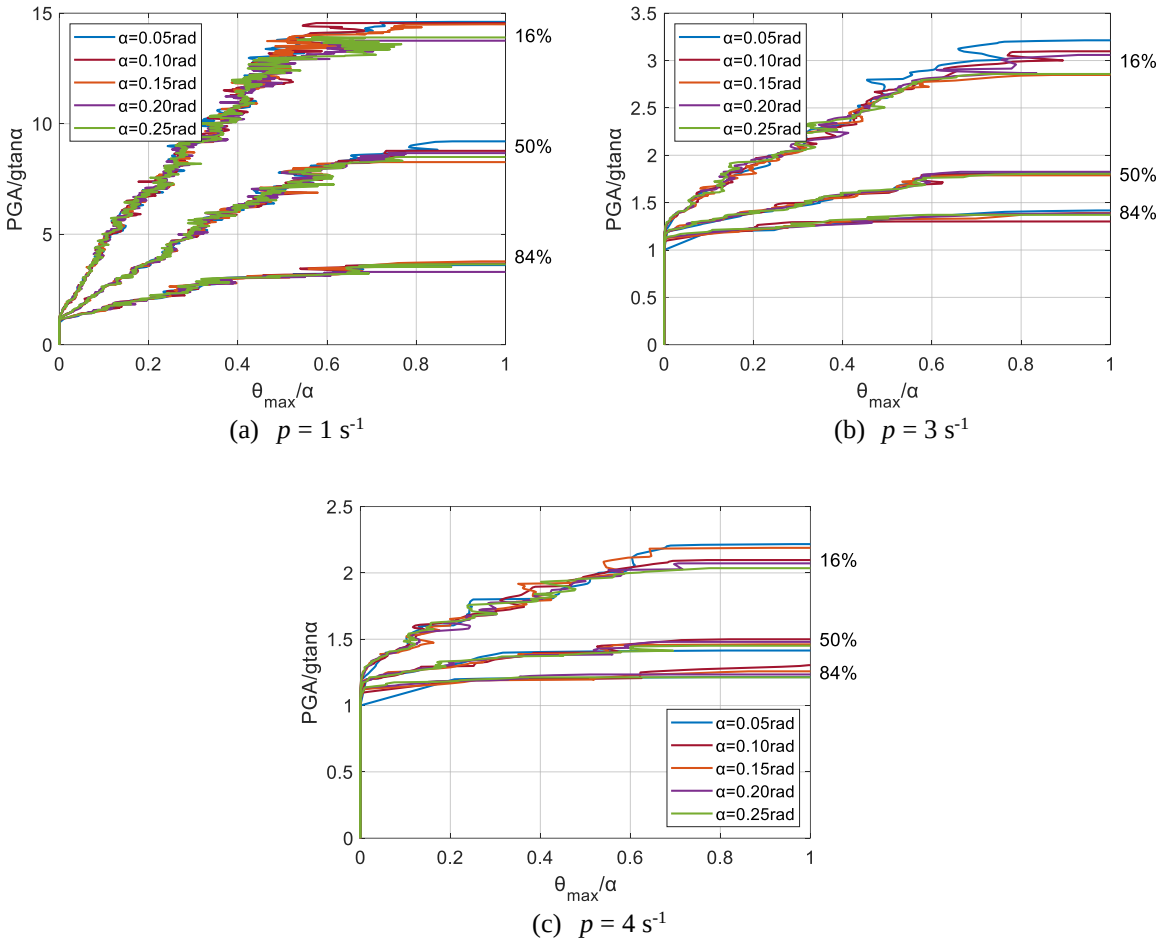

(a) p = 1 s^{-1} (b) p = 3 s^{-1}

(c) p = 4 s^{-1}

Figure 8. 16/50/84% EDP|IM IDA quantiles for blocks of different slenderness under 86 ordinary ground motions.

Record scaling versus block slenderness adjustment

The fourth stage is the ultimate test in advocating full normalization of rocking response by α; it is the determination of IDA-like curves without scaling the records, but rather by adjusting α itself. Conceptually, this is important as it requires no artificial modification of the as-recorded ground motion, only the aggregation of results coming from blocks with different slenderness (and the same p). It is directly equivalent to the derivation of IDAs in elastoplastic oscillators by reducing the yield strength rather than upscaling the ground motions. Whereas the latter is a time-honored practice whose validity has been mathematically proven for such simple systems [33, 55], the same cannot be said for rocking blocks. Still, our results so far empirically suggest that this should be doable. And it is. Figures 9 and 10 show an example comparison between IDA results for the blocks with α = 0.10 rad derived by scaling the 86 ordinary ground motions versus the alternative IDA-like curves with the same records in their unscaled form by adjusting the slenderness α at each dimensionless $PGA/\mathrm{g}\tan\alpha$ level. Specifically, in Figure 9 the ratios of $\tilde{\theta}$ per Equation (4) of the alternative IDA (*unscaled records*) versus the conventional IDA (*scaled records*) of the blocks with α = 0.10 rad are presented in boxplots. Again, only the well-defined ratios are included. As illustrated, for all the values of p the two approaches yield practically identical results under a paired record-by-record comparison in almost all the IM-levels. This fact is also observed when looking at the ensemble statistics (i.e., quantiles) in Figure 10 where the differences between the two methods are negligible. To this end, after this final comparison stage, one can say that even for the case of the ordinary ground motions, slenderness can be normalized out for rocking blocks when the seismic response is treated on a probabilistic basis. However, this conclusion only holds when η is constant and independent of the slenderness. As mentioned earlier, this would not be the case if one adopts the proposal of Housner [2], where η becomes a function of α.

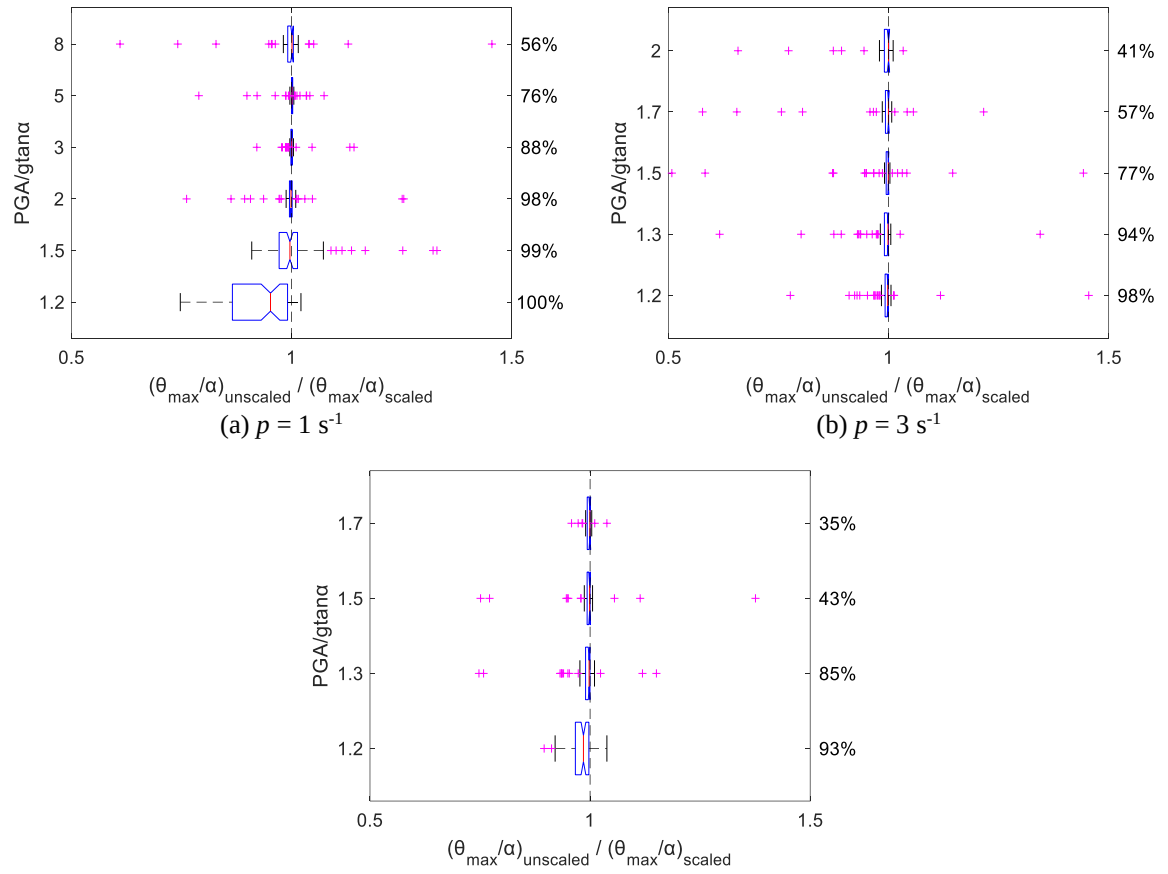

(a) p = 1 s^{-1} (b) p = 3 s^{-1}

(c) p = 4 s^{-1}

Figure 9. Boxplots of the record-per-record ratios of EDP derived via response-history analysis using slenderness-adjustment (unscaled record) over conventional same-slenderness (scaled record, α = 0.10 rad) results. The percentage of non-infinite ratios from 86 total appears on the right vertical edge for each intensity level.

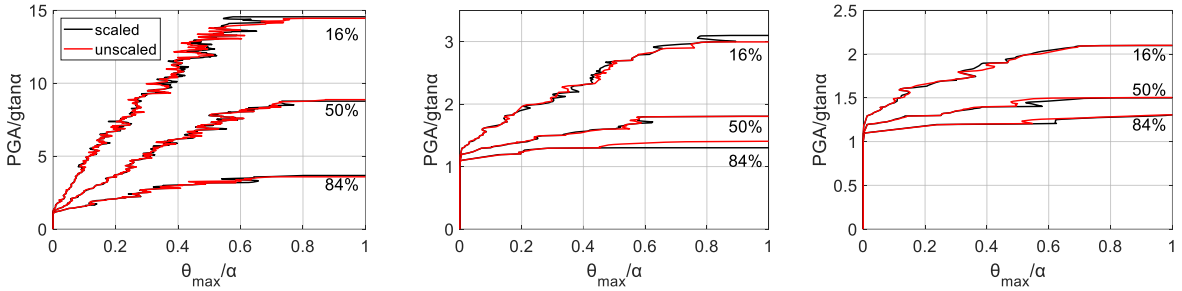

(a) p = 1 s^{-1} (b) p = 3 s^{-1} (c) p = 4 s^{-1}

Figure 10. 16/50/84% EDP|IM quantiles for IDA of blocks with α = 0.10 rad (scaled records) against the alternative IDA-like (unscaled records) procedure by adjusting the slenderness instead of scaling the ground motions, under 86 ordinary ground motions.

5 STATISTICAL CHARACTERIZATION OF ROCKING FRAGILITIES

Having resolved to our satisfaction the question of slenderness, we are now interested in characterizing the output distribution of the IM values corresponding to a given EDP. The respective cumulative distribution function (CDF) is essentially the fragility curve associated with the exceedance of the given EDP threshold. Fitting such rocking fragilities with a parametric distribution is desirable since it reduces an inherently random quantity to a handful of parameters, facilitating the treatment of the problem and the determination of fragilities. For yielding structural systems, the two-parameter lognormal distribution is almost universally considered a suitable choice for any EDP threshold [34–36, 57]. Thus, this will be our starting point. In addition, a shifted lognormal distribution will also be tested, employing a third parameter, IM_R, to shift the lognormal to the right (i.e., to higher values), essentially

extinguishing the probability of non-zero response for $IM < IM_R$, or in general before uplift occurs [58]. This is considered advantageous, as a classic lognormal distribution would predict some probability of non-zero response even before the actual initiation of rocking motion.

Lognormal versus shifted lognormal distribution

First, we determine the set of IM values that correspond to each EDP threshold, for multiple $\tilde{\theta}$ values ranging from 0 to 1 and each of the 15 rocking blocks of Table 1. Both the sets of 86 ordinary and 44 pulse-type ground motions are employed. Since the investigation is done on an IM|EDP basis and due to the highly weaving behavior of the typical rocking IDA curve, there can be multiple IMs that correspond to a single $\tilde{\theta}$ on a curve. Therefore, a functional inversion is needed to turn the IDA curves into one-to-one functions that provide a single IM for each given EDP. Here, the median-point inversion technique is employed, essentially using the median of the multiple IM values corresponding to any given EDP, this being a nearly unbiased approach for rocking IDAs [37].

Figure 11 presents the inverted IDAs for the block with α = 0.20 rad, p =1 s^{-1} under the set of 86 ordinary ground motions for the dimensionless *PGA* (Figure 11a) and *PGV* (Figure 11b). As illustrated in Figure 11a, the onset of rocking is clearly demarcated for the dimensionless *PGA*. This is due to the uplift condition being exactly $PGA > \mathrm{g}\tan\alpha$, or $PGA/\mathrm{g}\tan\alpha > 1$. Thus, fitting a lognormal distribution to $PGA/\mathrm{g}\tan\alpha - IM_R$, where $IM_R = 1$, is only natural. In proper probabilistic terminology, this is equivalent to fitting a lognormal distribution (right-)shifted by IM_R. On the other hand, for the case of the dimensionless *PGV* there is no such clear uplift criterion, leading to the hazier view of Figure 11b. For simplicity, we employ as IM_R the lowest value of $pPGV/\mathrm{g}\tan\alpha$ to trigger rocking for the given set of records.

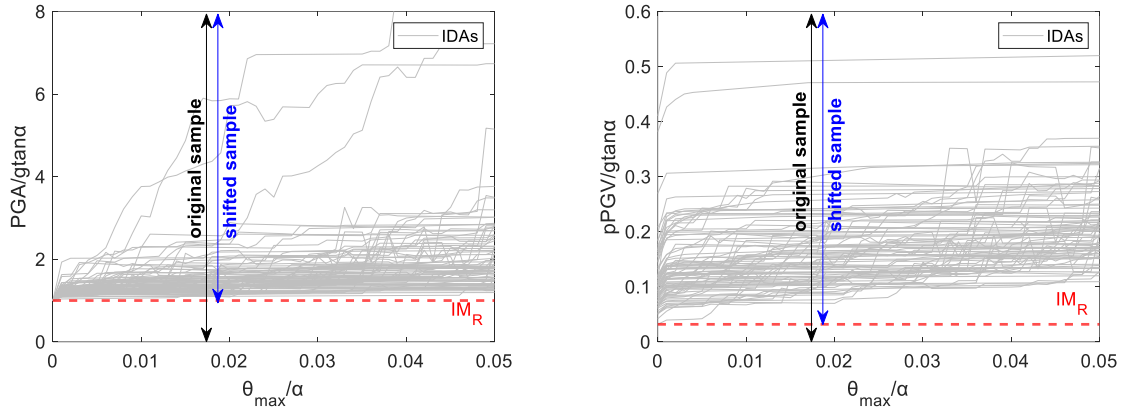

(a) $PGA/\mathrm{g}\tan\alpha$ (b) $pPGV/\mathrm{g}\tan\alpha$

Figure 11. Original vis-à-vis shifted sample of the IM|EDP IDA curves (inverted using the median-point-along-the-vertical technique [37]) under 86 ordinary ground motions. Block with p = 1 s^{-1}, α = 0.20 rad.

The Lilliefors [59] test is employed to check for lognormality, both for the unshifted and the shifted distribution. Figure 12 presents the results for the case of the dimensionless *PGA* summarized into the percentage of the $\tilde{\theta}$ range where lognormality is an acceptable assumption at the 5% significance level. As illustrated, lognormality is not an adequate model when the original (unshifted) sample of the IM values is used both for the ordinary and the pulse-type ground motions, especially when the small blocks (i.e., higher p values) are considered. On the other hand, shifting enhances the fit of the lognormal distribution in the full range of rocking response, even if not reaching 100% for some cases. To further investigate some badly performing cases, Figure 13 displays the Lilliefors test results for the full range of response for two of the blocks with p = 3 s^{-1}. In Figure 13a, the block with α = 0.05 rad shows non-lognormal behavior for the full range of response, both for the original and the shifted sample. The reason is made clearer when comparing the histograms of the original and the shifted sample at a specific $\tilde{\theta}$ level ($\tilde{\theta} = 0.50$) in Figures 13b-13c: shifting clearly results to a better approximation of the normal distribution for the natural logarithm of the IM values. However, for this slender block there are some records that produce overturning for intensities that are very close to uplift, and specifically very close to IM_R. These become outliers to the left of the IM sample, precluding any applicability of the lognormal distribution. On the other hand, for the case of the less slender block with α = 0.20 rad (Figures 13d-f), the absence of these early-overturning cases leads to a better fit. Overall, the shifted-lognormal (and to a lesser extent the lognormal), are an acceptable but imperfect assumption for the case of the rocking fragilities when *PGA* or its dimensionless form are employed as the IM.

Considering the *PGV*, the summarized results of the Lilliefors tests are presented in Figure 14. As shown, the lognormal distribution is a much better fit now. Even the original sample is fitted successfully for more than 70% of the full range of response for most of the blocks. Shifting improves this to over 90%.

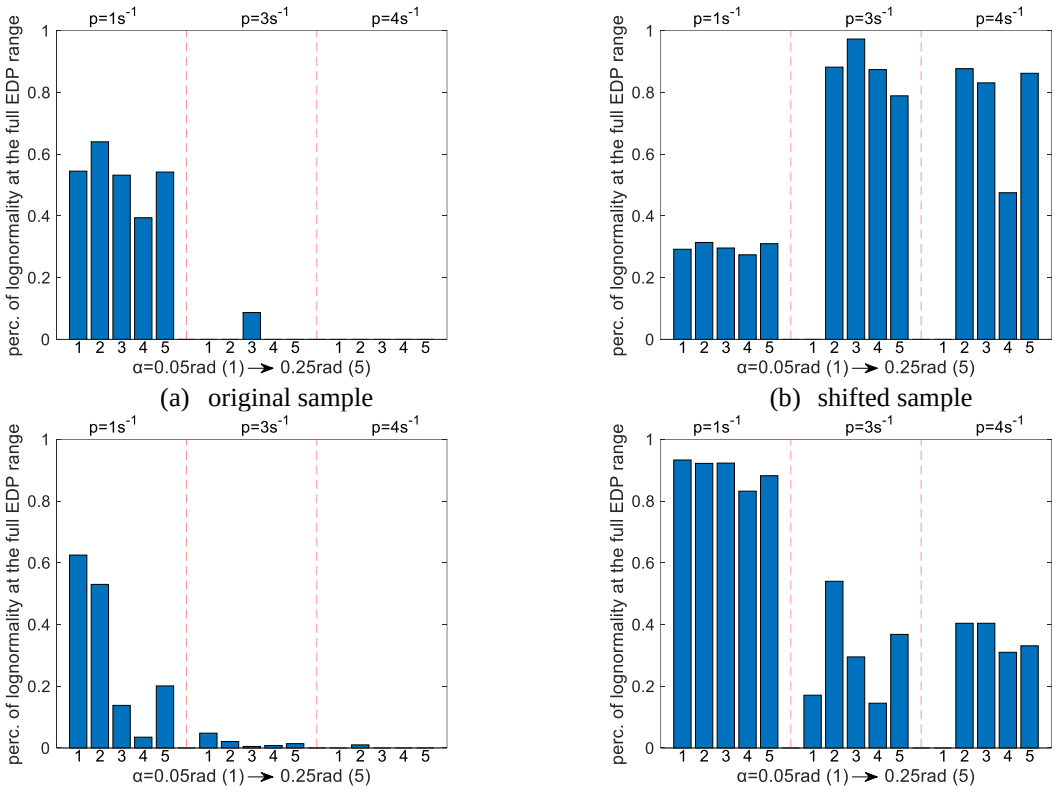

(a) original sample (b) shifted sample

(c) original sample (d) shifted sample

Figure 12. Summarized Lilliefors test results for the IM|EDP IDAs for $PGA/\mathrm{g}\tan\alpha$, using $\alpha = 0.05,\ldots,0.25$ rad: (a)-(b) 86 ordinary ground motions, (c)-(d) 44 pulse-type ground motions.

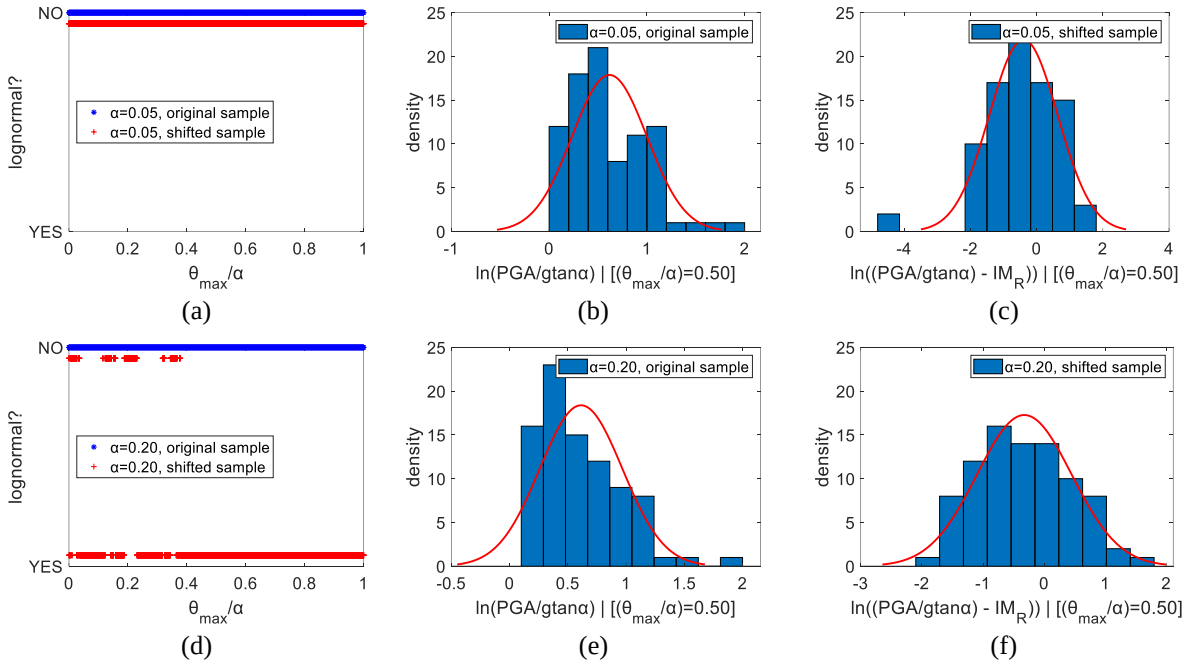

(a) (b) (c)

(d) (e) (f)

Figure 13. Lilliefors tests for blocks with $p = 3\mathrm{s}^{-1}$ using a sample of 86 ordinary ground motions. (a)-(c) Block with $\alpha = 0.05$ rad, (d)-(f) block with $\alpha = 0.20$ rad.

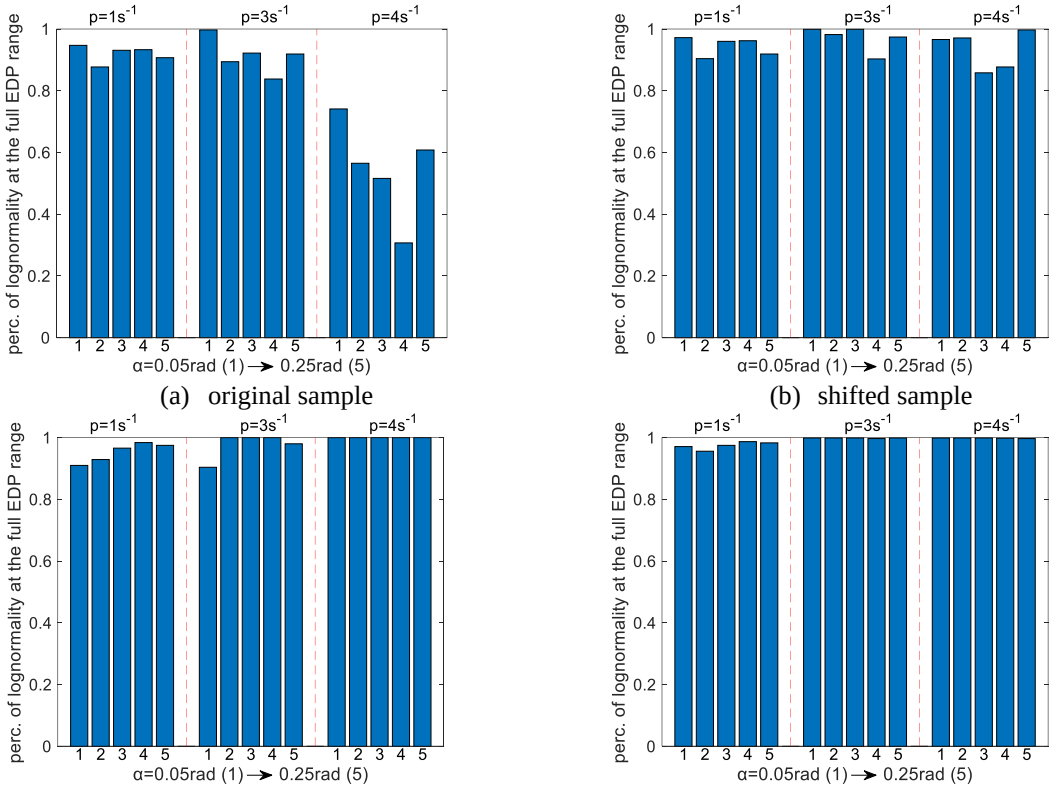

(a) original sample (b) shifted sample

(c) original sample (d) shifted sample

Figure 14. Summarized Lilliefors test results for the IM|EDP IDA curves for $pPGV/g\tan\alpha$, using α = 0.05,…,0.25 rad: (a)-(b) 86 ordinary ground motions, (c)-(d) 44 pulse-type ground motions.

Rocking response distribution and fragility estimations

Based on the above findings, the question is how to take advantage of a shifted (three-parameter) or an unshifted (two-parameter) lognormal distribution to achieve a parametric description of rocking fragilities. This pertains to the practical problem of optimally fitting rocking response prediction equations [31, 39]. The following three options are considered as potential candidates:

1. Shift the empirical IM capacity data. Estimate their median and dispersion. Provide regression relationships for the shift (if it is non-obvious), the median, and the dispersion.
2. Do not shift the empirical IM capacity data. Estimate their 16/50/84 percentile values. Provide regression relationships for the percentile values. Offer a transformation to allow their shifting, if needed.
3. Do not shift the empirical IM capacity data. Estimate their median and dispersion. Offer a transformation to allow their shifting, if needed.

The first approach seems like the obvious winner. It perfectly follows our findings and uses the shifted lognormal as a basis. This is its greatest advantage but at the same time its worst detriment. The reason is that a shifted lognormal is not intuitive to many users, while popular risk/loss assessment frameworks, such as FEMA P-58 [60], are based on unshifted normal and lognormal distributions by default. In other words, unless one wants to rewrite the PACT software [60], Option 1 is a no go. Moreover, it needs three regressions for the dimensionless *PGV*, although only two for the case of the dimensionless *PGA* having a constant $IM_R = 1$. Option 2 is a potentially much better choice. It follows the paradigm of SPO2IDA [29] and by directly fitting quantiles it is fully distribution free. If a new study comes out that claims a certain two/three-parameter distribution is better than a shifted lognormal, then one can still use the three expressions developed via Option 2 to fit it. The only disadvantage for the present-day analyst is that three regressions are more difficult than two especially for the case of the rocking block. Whereas SPO2IDA could capitalize on the fact that the same parametric expression could be employed for all three quantiles of yielding oscillators (with different fitted coefficients naturally), this is not necessarily the case for rocking systems. The sizeable record-to-record variability can make the 16/84% quantiles quite temperamental and difficult to capture. This is where Option 3 shines: by virtue of ignoring the 16/84% quantiles and going directly for the more stable dispersion as a parameter, it makes it easier to achieve a good fit. For this reason, Option 3 became the approach of choice for Kazantzi *et al.* [31, 39].

Still, it would be attractive to be able to combine the best of both worlds. Using Option 2 or 3 allows us to directly fit an unshifted lognormal, retaining full compatibility with FEMA P-58. Having the capability to transition to a shifted lognormal while reusing the same fitted expressions, would also give us the opportunity to increase fidelity without cost. Shifting by IM_R the original sample of data is actually a fairly tractable operation. In the case of Option 2, the 16/50/84% fractiles of the original sample are directly shifted by IM_R as well. Thus, the logarithmic mean (μ_s) and dispersion (β_s) of a shifted lognormal distribution can be calculated from the 16/50/84% fractiles ($IM_{16}^o, IM_{50}^o, IM_{84}^o$) of the original sample as:

$$\mu_s = \ln(IM_{50}^o - IM_R) \tag{5}$$

$$\begin{aligned} \beta_s &= 0.5(\ln IM_{84}^s - \ln IM_{16}^s) \\ &= 0.5[\ln(IM_{84}^o - IM_R) - \ln(IM_{16}^o - IM_R)] \end{aligned} \tag{6}$$

If, on the other hand, we only have the dispersion β_o of the original unshifted datapoints per Option 2, we need to at least assume that the unshifted data "satisfactorily" follows a lognormal distribution. This is not exactly ideal, given that it is this particular distribution that we are trying to escape, but it is the only available path. Then, the dispersion be approximated in log-space by taking 1/(2c) times the difference of two "reference" points in log-space at ±c standard deviations from the median:

$$\begin{aligned} \beta_s &= \frac{1}{2c}\left[\ln\left(IM_{50}^o e^{c\beta_o} - IM_R\right) - \ln\left(IM_{50}^o e^{-c\beta_o} - IM_R\right)\right] \\ &= \frac{1}{2c}\left[\ln\left(\frac{IM_{50}^o e^{c\beta_o} - IM_R}{IM_{50}^o e^{-c\beta_o} - IM_R}\right)\right] \end{aligned} \tag{7}$$

The constant c can theoretically range in (0, +∞). A typical choice could be c = 1, which corresponds to having the two "reference" points at standard deviation away from the median, making them equivalent to the 16/84% values and yielding back Equation (6). Still, there are two practical issues to consider here. First, it often happens that using MLE or moment-fitting on the full original sample can lead to an overestimation of β_o. This is due to a propensity of the sample towards having a long right tail, thus pulling the dispersion to large values. Combined with a relatively large value of c, this can make the denominator of Equation (7) approach zero (or even become negative) adversely impacting (or fully negating) the assessment of the shifted sample dispersion. Thus, it is usually better if (i) the right tail of the original (unshifted) sample is trimmed before fitting, and (ii) c stays within [0.5, 1]. For example, if using MLE, one may choose to discard observations beyond the 95% value; for moment-fitting, one can either estimate dispersion β_o as the half distance between IM_{16}^o and IM_{84}^o, or take the standard deviation of the natural logarithm of the data after similarly discarding observations above the 95% value.

As an example, the different options are compared in terms of the fragility functions in Figures 15–17. All the results refer to the block with p = 3 s^{-1} and α = 0.20 rad. Three different EDP thresholds are defined: $\tilde{\theta} = 0.15, 0.35, 1.00$ [51]. For each case, there are four different fragility candidates to consider

- Empirical cumulative distribution function (ECDF) fragility: Determined as an empirical CDF on a vertical-statistics basis using the sample of 86 IM points from the set of ordinary ground motions, as determined via the median-point-along-the-vertical inversion technique [37]. This is the unambiguous benchmark against which all other options should be compared.
- Unshifted-sample-fitted lognormal (USFL) fragility: The lognormal distribution CDF fitted on the original unshifted sample of the 86 IM points employed for the ECDF fragilities.
- Shifted-sample-fitted lognormal (SSFL) fragility: The lognormal distribution CDF fitted on the shifted sample of the 86 IM points.
- Transformed via Equation (7) USFL (USFL7) fragility: The result of transforming (shifting) the USFL fragility by applying Equation (7), and of course Equation (5).

Figures 15a-b, present for the dimensionless *PGA* and *PGV*, respectively, the ECDF fragilities versus their USFL (solid lines) and SSFL (dashed lines) counterparts. The latter are fitted via maximum likelihood estimation (MLE [61]) without tail-trimming. The results shown offer unambiguous support to the findings of the previous subsection: fitting a lognormal to the shifted *PGA* data offers a substantially better model (Figures 15a), fully capturing the deterministic initiation of rocking uplift, while it is only a marginal improvement for *PGV*. Of course, such results are only attainable if we have the full sample available.

Let us now see how this situation may change if we only have the sample statistics per the theoretically-weaker Option 3. Figures 16a-b compare for *PGA* and *PGV*, respectively, the ECDF fragilities against USFL (solid lines) and USFL7 (dashed lines) fragilities, both determined using a trimmed-sample moment-fit approach with c = 1.

As expected, everything is working well for the *PGV* in Figure 16b. The original data is already well-represented by a lognormal, satisfying the assumptions of Option 3. The transformation of the fitted parameters again marginally improves an already good fit, same as in Figure 15b. For the *PGA*, the USFL remains a bad choice, as it misses the uplift threshold of $PGA/(\mathrm{g}\tan\alpha) = 1$. Despite somewhat violating the need for a "lognormality of unshifted data", Equation (7) manages a good job of transforming the USFL results to USFL7 fragilities. Although the latter do not fully match the right tail at overturning ($\tilde{\theta} = 1.0$), they do offer a close enough fit. After all, this is the part that is of least consequence for the seismic risk, as it concerns rare ground motions and low hazards.

While the trimmed-sample fit provides good results per Figure 16, this is not necessarily the case for an untrimmed-sample in Figure 17. Specifically, Figures 17a-b offer for *PGA* and *PGV*, respectively, said USFL fragilities fitted by MLE together with their corresponding USFL7 curves derived via Equation (7) for $c = 1$. Once again, the results are of no concern for *PGV*. For *PGA*, though, shifting an untrimmed-sample fragility by Equation (7) fails to produce an effective match.

The effect of trimming versus no trimming the data sample appears more clearly in Figure 18. Therein, only the troublesome *PGA* results are shown, featuring the SSFL (benchmark) fragilities against 4 different cases of USFL7, using untrimmed (Figure 18a) versus trimmed (Figure 18b) sample fitting. As illustrated, a low value of c=0.25–0.5 can help improving the USFL7 result even for an untrimmed sample. Still, if trimming is well-performed, practically any value of c = 0.25–1 will provide more-or-less the same result.

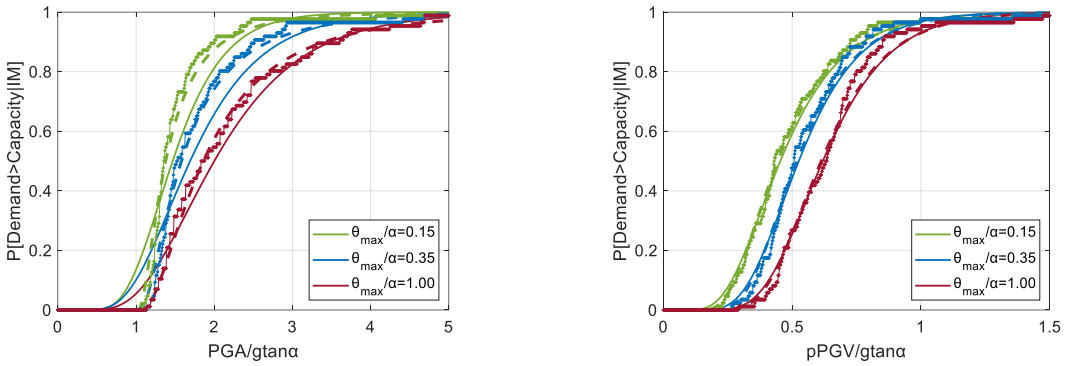

(a) (b)

Figure 15. Fragility functions for 3 pre-defined $\tilde{\theta}$ thresholds and 86 ordinary records. Block with p = 3 s^{-1}, α = 0.20 rad. ECDF fragilities (solid line plus dots) vis-à-vis USFL (untrimmed-sample: solid line) and the corresponding SSFL (dashed lines) fragilities.

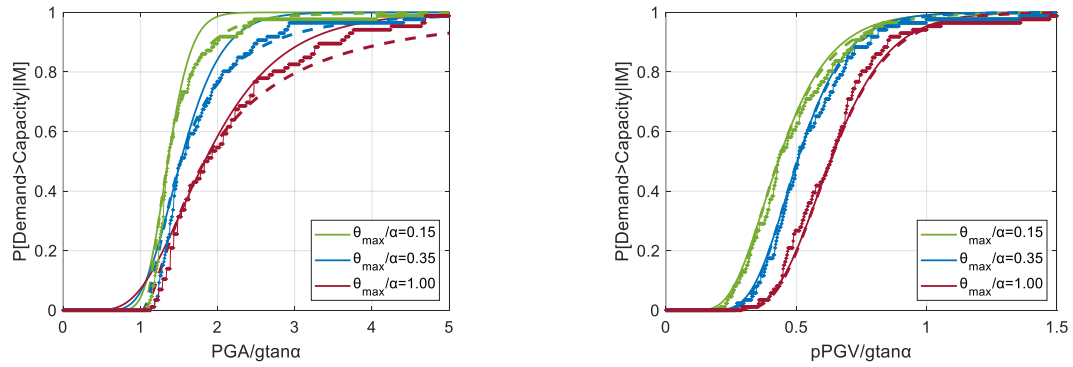

(a) (b)

Figure 16. Fragility functions for 3 pre-defined $\tilde{\theta}$ thresholds and 86 ordinary records. Block with p = 3 s^{-1}, α = 0.20 rad. (a)-(b) ECDF fragilities (solid line plus dots) vis-à-vis the USFL (trimmed-sample: solid line) and corresponding USFL7 (dashed line) fragilities for c = 1.

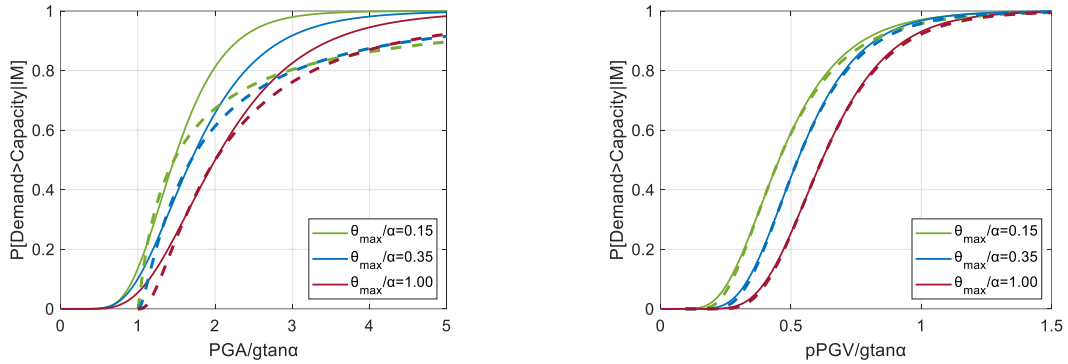

Figure 17. Fragility functions for 3 pre-defined $\tilde{\theta}$ thresholds and 86 ordinary records. Block with p = 3 s^{-1}, α = 0.20 rad. (a)-(b) USFL (untrimmed-sample: solid line) vis-à-vis the corresponding USFL7 (dashed line) fragilities for c = 1.

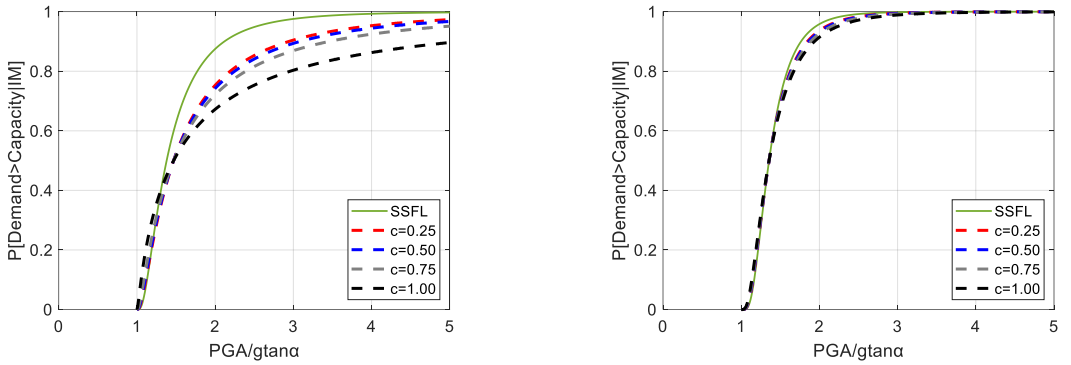

Figure 18. Fragility functions for the $\tilde{\theta} = 0.15$ threshold and 86 ordinary records. Block with p = 3 s^{-1}, α = 0.20 rad. SSFL (solid lines) vis-à-vis the corresponding (a) USFL7 (untrimmed-sample: dashed line) fragilities, (b) USFL7 (trimmed-sample: dashed line) fragilities.

6 CONCLUSIONS

A detailed investigation of the influence of the system parameters on the probabilistic treatment of the rocking seismic response is presented. It is found that the slenderness (or stability) angle (α) can be normalized out of the problem when using dimensionless intensity and response variables and assuming a constant (α-independent) value for the coefficient of restitution. This normalization is shown to work efficiently for the relatively slender rocking blocks ($\alpha \leq 0.25$ rad) under both pulse-type and ordinary ground motions; extension to stockier blocks seems probable, but will need to be explored in future studies. Furthermore, this study has offered a comprehensive investigation on the rocking probability distribution. A lognormal assumption can be employed for the case of the rocking fragilities when *PGA* or *PGV* are used as IMs, despite mostly lacking in statistical significance for the former. If a better probabilistic model is sought, a lognormal that is shifted to provide zero probability before the initiation of rocking offers an unambiguous improvement. All these findings support the treatment of rocking under a statistical view for the purposes of seismic design and assessment.

ACKNOWLEDGEMENTS

This research has been co-financed by the European Regional Development Fund of the European Union and Greek national funds through the Operational Program Competitiveness, Entrepreneurship and Innovation, under the call RESEARCH – CREATE – INNOVATE (project code: T1EDK-00956), project: "ARCHYTAS: Archetypal telemetry and decision support system for the protection of monumental structures". Financial support has been also provided by the European Framework Programme for Research and Innovation (Horizon 2020) under the "HYPERION" project with Grant Agreement number 821054. The authors would like to thank Dr M.F. Vassiliou for providing the MATLAB script for undertaking the numerical study on the rocking oscillators under earthquake excitations.

FUNDING INFORMATION

This research has been co-financed by the European Regional Development Fund of the European Union and Greek national funds through the Operational Program Competitiveness, Entrepreneurship and Innovation, under the call RESEARCH – CREATE – INNOVATE (project code: T1EDK-00956), project: "ARCHYTAS: Archetypal telemetry and decision support system for the protection of monumental structures". Financial support has been also provided by the European Framework Programme for Research and Innovation (Horizon 2020) under the "HYPERION" project with Grant Agreement number 821054.

REFERENCES

[1] Giouvanidis AI, Dimitrakopoulos EG. Nonsmooth dynamic analysis of sticking impacts in rocking structures. *Bulletin of Earthquake Engineering* 2017; **15** (5): 2273–2304. https://doi.org/10.1007/s10518-016-0068-4

[2] Housner GW. The behavior of inverted pendulum structures during earthquakes. *Bulletin of the Seismological Society of America*, 1963;**53**(2):403–417.

[3] Yim C-S, Chopra AK, Penzien J. Rocking response of rigid blocks to earthquakes. *Earthquake Engineering and Structural Dynamics*, 1980;**8**(6):565–587. https://doi.org/10.1002/eqe.4290080606

[4] Ishiyama Y. Motions of rigid bodies and criteria for overturning by earthquake excitations. *Earthquake Engineering and Structural Dynamics*, 1982;**10**(5):635–650. https://doi.org/10.1002/eqe.4290100502

[5] Spanos A, Koh S. Rocking of Rigid blocks due to harmonic shaking. *Journal of Engineering Mechanics ASCE*, 1984;**110**(11):1627–1642. https://doi.org/10.1061/(ASCE)0733-9399(1984)110:11(1627)

[6] Makris N, Roussos Y. Rocking response of rigid blocks under near-source ground motions. *Géotechnique*, 2000; **50**(3):243–262. https://doi.org/10.1680/geot.2000.50.3.243

[7] Zhang J, Makris N. Rocking response of free-standing blocks under cycloidal pulses. *Journal of Engineering Mechanics (ASCE)* 2001;**127**(5):473–483. https://doi.org/10.1061/(ASCE)0733-9399(2001)127:5(473)

[8] Makris N, Konstantinidis D. The rocking spectrum and the limitations of practical design methodologies. *Earthquake Engineering and Structural Dynamics*, 2003;**32**(2):265–289. https://doi.org/10.1002/eqe.223

[9] Vassiliou MF, Makris N. Analysis of the rocking response of rigid blocks standing free on a seismically isolated base. *Earthquake Engineering and Structural Dynamics*, 2012;**41**(2):177–196. https://doi.org/10.1002/eqe.1124

[10] Dimitrakopoulos EG, DeJong MJ. Revisiting the rocking block: closed-form solutions and similarity laws. *Proceedings of the Royal Society A: Mathematical, Physical and Engineering Sciences*, 2012;**468**(2144):2294–2318. https://doi.org/10.1098/rspa.2012.0026

[11] Makris N, Vassiliou MF. Planar rocking response and stability analysis of an array of free-standing columns capped with a freely supported rigid beam. *Earthquake Engineering and Structural Dynamics*, 2013;**42**(3):431–449. https://doi.org/10.1002/eqe.2222

[12] Voyagaki E, Psycharis IN, Mylonakis G. Rocking response and overturning criteria for free standing rigid blocks to single-lobe pulses. *Soil Dynamics and Earthquake Engineering*, 2013;**46**:85–95. https://doi.org/10.1016/j.soildyn.2012.11.010

[13] Dimitrakopoulos EG, Paraskeva TS. Dimensionless fragility curves for rocking response to near-fault excitations. *Earthquake Engineering and Structural Dynamics*, 2015;**44**(12):2015–2033. https://doi.org/10.1002/eqe.2571

[14] Dimitrakopoulos EG, Fung EDW. Closed-form rocking overturning conditions for a family of pulse ground motions. *Proceedings of the Royal Society A: Mathematical, Physical and Engineering Sciences*, 2016;**472**(2196):20160662. https://doi.org/10.1098/rspa.2016.0662

[15] Makris N, Kampas G. Size versus slenderness: two competing parameters in the seismic stability of free-standing rocking columns. *Bulletin of the Seismological Society of America*, 2016;**106**(1):104. http://dx.doi.org/10.1785/0120150138

[16] Bachmann JA, Strand M, Vassiliou MF, Broccardo M, Stojadinović B. Is rocking motion predictable? *Earthquake Engineering and Structural Dynamics*, 2018;**47**(2):535–552. https://doi.org/10.1002/eqe.2978

[17] Psycharis IN, Papastamatiou DY, Alexandris AP. Parametric investigation of the stability of classical columns under harmonic and earthquake excitations. *Earthquake Engineering and Structural Dynamics*, 2000;**29**(8):1093–1109. https://doi.org/10.1002/1096-9845(200008)29:8<1093::AID-EQE953>3.0.CO;2-S

[18] Mouzakis HP, Psycharis IN, Papastamatiou DY, Carydis PG, Papantonopoulos C, Zambas C. Experimental investigation of the earthquake response of a model of a marble classical column. *Earthquake Engineering and Structural Dynamics*. 2002;**31**(9):1681–1698. https://doi.org/10.1002/eqe.184

[19] Papantonopoulos C, Psycharis IN, Papastamatiou DY, Lemos JV, Mouzakis HP. Numerical prediction of the earthquake response of classical columns using the distinct element method. *Earthquake Engineering and Structural Dynamics*. 2002;**31**(9):1699–1717. https://doi.org/10.1002/eqe.185

[20] Nikolić Ž, Krstevska L, Marović P, Smoljanović H. Experimental investigation of seismic behaviour of the ancient Protiron monument model. *Earthquake Engineering and Structural Dynamics*. 2019;**48**(6):573–593. https://doi.org/10.1002/eqe.3149

[21] Giouvanidis AI, Dong Y. Seismic loss and resilience assessment of single-column rocking bridges. *Bulletin of earthquake engineering*. 2020;**18**:4481–4513. https://doi.org/10.1007/s10518-020-00865-5

[22] Manzo NR, Vassiliou, MF. Cyclic tests of a precast restrained rocking system for sustainable and resilient seismic design of bridges. *Engineering Structures*. 2021;113620. https://doi.org/10.1016/j.engstruct.2021.113620

[23] Ríos-García G, Benavent-Climent A. New rocking column with control of negative stiffness displacement range and its application to RC frames. *Eng Struct*. 2020;**206:**110133. https://doi.org/10.1016/j.engstruct.2019.110133

[24] Agalianos A, Psychari A, Vassiliou MF, Stojadinovic B, Anastasopoulos I. Comparative assessment of two rocking isolation techniques for a motorway overpass bridge. *Front Built Environ*. 2017;**3**:47. https://doi.org/10.3389/fbuil.2017.00047

[25] Voyagaki E, Vamvatsikos D. Probabilistic assessment of rocking response for simply-supported rigid blocks. SECED 2015 Conference: Earthquake Risk and Engineering towards a Resilient World, Cambridge UK, 2015.

[26] Vassiliou, MF, Broccardo, M, Cengiz, C, et al. Shake table testing of a rocking podium: Results of a blind prediction contest. *Earthquake Engng Struct Dyn*. 2021; 50: 1043– 1062. https://doi.org/10.1002/eqe.3386

[27] Zhong, C, Christopoulos, C. Finite element analysis of the seismic shake-table response of a rocking podium structure. *Earthquake Engng Struct Dyn*. 2021; 50: 1223– 1230. https://doi.org/10.1002/eqe.3397

[28] Veletsos AS, Newmark NM. Effect of inelastic behavior on the response of simple systems to earthquake motions, Proc., 2nd World Conference on Earthquake Engineering, Japan, Vol. 2, 895–912, 1960.

[29] Vamvatsikos D, Cornell CA. Direct estimation of the seismic demand and capacity of oscillators with multilinear static pushovers through Incremental Dynamic Analysis. *Earthquake Engineering and Structural Dynamics*, 2006;**35**(9):1097–1117. https://doi.org/10.1002/eqe.573

[30] Ruiz-Garcia J, Miranda E. Probabilistic estimation of maximum inelastic displacement demands for performance-based design. *Earthquake Engineering and Structural Dynamics*, 2007;**36**(9):1235–1254. https://doi.org/10.1002/eqe.680

[31] Kazantzi AK, Lachanas CG, Vamvatsikos D. Seismic response distribution expressions for on-ground rigid rocking blocks under ordinary ground motions. *Earthquake Engineering and Structural Dynamics*, 2021;**50**(12):3311–3331 https://doi.org/10.1002/eqe.3511

[32] Bakalis K, Vamvatsikos D. Seismic fragility functions via nonlinear response history analysis. *Journal of Structural Engineering (ASCE)*. 2018;**144**(10):04018181. https://doi.org/10.1061/(ASCE)ST.1943-541X.0002141

[33] Miranda, E. Evaluation of site-dependent inelastic seismic design spectra. *Journal of Structural Engineering*, 1993;**119**(5):1319–1338. https://doi.org/10.1061/(ASCE)0733-9445(1993)119:5(1319)

[34] Romão X, Delgado R, Costa A. Assessment of the Statistical Distributions of Structural Demand Under Earthquake Loading. *Journal of Earthquake Engineering*. 2011;**15**:(5):724–753. https://doi.org/10.1080/13632469.2010.539296

[35] Goda K, Hong HP, Lee CS. Probabilistic characteristics of seismic ductility demand of SDOF systems with Bouc-Wen hysteretic behaviour," *Journal of Earthquake Engineering* 2009;**13**(5):600–622. https://doi.org/10.1080/13632460802645098

[36] Shinozuka M, Feng MQ, Lee J, Naganuma T. (2000). Statistical analysis of fragility curves. *Journal of engineering mechanics*, 2000;**126**(12):1224–1231. https://doi.org/10.1061/(ASCE)0733-9399(2000)126:12(1224)

[37] Lachanas CG, Vamvatsikos D. Rocking incremental dynamic analysis. *Earthquake Engineering and Structural Dynamics*, 2022;**51**(3):688–703. https://doi.org/10.1002/eqe.3586

[38] Lachanas CG, Vamvatsikos D, Vassiliou MF. The influence of the vertical component of ground motion on the probabilistic treatment of the rocking response of free-standing blocks. *Earthquake Engineering and Structural Dynamics*, 2022. https://doi.org/10.1002/eqe.3643

[39] Kazantzi AK, Lachanas CG, and Vamvatsikos D. Seismic response distribution expressions for rocking building contents under ordinary ground motions. *Bulletin of Earthquake Engineering*, 2022;20:6659–6682. https://doi.org/10.1007/s10518-022-01424-w

[40] Lachanas CG, Vamvatsikos D, Dimitrakopoulos EG (2022). Intensity measures as interface variables versus response proxies: the case of rocking blocks. *Earthquake Engineering and Structural Dynamics.* [under review]

[41] Lachanas CG, Vamvatsikos D. Preliminary seismic risk assessment of ancient columns across Attica for application in decision support systems." *Proc., 3rd European Conference on Earthquake Engineering & Seismology*, Bucharest, Romania, 2022.

[42] Priestley MJN, Evison RJ, Carr AJ. Seismic response of structures free to rock on their foundations. *Bulletin of the New Zealand National Society for Earthquake Engineering*. 1978;**11**(3):141–150. https://doi.org/10.5459/bnzsee.11.3.141-150

[43] Pena F, Prieto F, Lourenco PB, Campos Costa A, Lemos JV. On the dynamic of rocking motion of single rigid-block structures. *Engineering and Structural Dynamics.* 2007;**36**(15):2383–2399. https://doi.org/10.1002/eqe.739

[44] ElGawady MA, Ma Q, Butterworth JW, Ingham J. Effects of interface material on the performance of free rocking blocks. *Earthquake Engineering and Structural Dynamics*. 2011;**40**(4):375–392. https://doi.org/10.1002/eqe.1025

[45] Kalliontzis D, Sritharan S, Schultz A. Improved coefficient of restitutions estimation for free rocking members. *Journal of Structural Engineering*. 2016;**142**(12):06016002. https://doi.org/10.1061/(ASCE)ST.1943-541X.0001598

[46] Ceh N, Jelenic G, Bicanic N. Analysis of restitution in rocking of single rigid blocks. *Acta Mechanica*. 2018;229: 4623–4642. https://doi.org/10.1007/s00707-018-2246-8

[47] Giouvanidis AI, Dimitrakopoulos EG. Seismic performance of rocking frames with flag-shaped hysteretic behavior. *Journal of Engineering Mechanics (ASCE).* 2017;**143**(5):04017008. https://doi.org/10.1061/(ASCE)EM.1943-7889.0001206

[48] Giouvanidis AI, Dimitrakopoulos EG. Rocking amplification and strong-motion duration. *Earthquake Engineering and Structural Dynamics*. 2018;**47**(10):2094–2116. https://doi.org/10.1002/eqe.3058

[49] DeJong MJ, Dimitrakopoulos EG. Dynamically equivalent rocking structures. *Earthquake engineering & structural dynamics* 2014;43 (10), 1543–1563. https://doi.org/10.1002/eqe.2410

[50] Makris N, Black CJ. Evaluation of peak ground velocity as a 'good' intensity measure for near-source ground motions. *Journal of Engineering Mechanics* (ASCE) 2004;**130**(9):1032–1044. https://doi.org/10.1061/(ASCE)0733-9399(2004)130:9(1032)

[51] Psycharis IN, Fragiadakis M, Stefanou I. Seismic reliability assessment of classical columns subjected to near-fault ground motions. *Earthquake Engineering and Structural Dynamics*. 2013;**42**(14):2061–2079. https://doi.org/10.1002/eqe.2312

[52] Vassiliou MF. Script for the seismic response of a planar rocking block, MATLAB script: available at http://hdl.handle.net/20.500.11850/521016, http://dx.doi.org/10.3929/ethz-b-000521016 last accessed April 2022.

[53] Chiou B, Darragh R, Gregor N, Silva W. NGA Project Strong-Motion Database. *Earthquake Spectra*, 2008;**24**(1): 23–44. http://dx.doi.org/10.1193/1.2894831

[54] Shahi SK, Baker JW. An efficient algorithm to identify strong velocity pulses in multi-component ground motions. *Bulletin of the Seismological Society of America.* 2014;**104**(5):2456–2466. https://doi.org/10.1785/0120130191

[55] Vamvatsikos D, Cornell CA. Incremental dynamic analysis. *Earthquake Engineering and Structural Dynamics* 2002;**31**(3):491–514. https://doi.org/10.1002/eqe.141

[56] McGill R, Tukey JW, Larsen WA. Variations of Boxplots. *The American Statistician*. 1978;**32**(1):12–16.

[57] Cornell CA, Krawinkler H. Progress and challenges in seismic performance assessment. PEER Center News 3 2000;(2):1–4.

[58] Stoica M, Medina RA, McCuen RH. Improved probabilistic quantification of drift demands for seismic evaluation. *Structural Safety*. 2007;**29**(2)132–145. https://doi.org/10.1016/j.strusafe.2006.03.003

[59] Lilliefors, H. W. On the Kolmogorov-Smirnov test for normality with mean and variance unknown. *Journal of the American Statistical Association*. 1967;**62**(318):399–402. https://doi.org/10.2307/2283970

[60] FEMA. *Seismic Performance Assessment of Buildings*. FEMA P-58, prepared by the Applied Technology Council for the Federal Emergency Management Agency, Washington, D.C. 2012

[61] Baker J W. Efficient analytical fragility function fitting using dynamic structural analysis. *Earthquake Spectra*. 2015;**31**(1):579–599. https://doi.org/10.1193/021113EQS025M